A NEW NEUTRON SPECTROMETRY SYSTEM FOR IN-CORE AND OUT-CORE APPLICATION AT WWER

H.-C. MEHNER, B. BÜHMER, U. HAGEMANN, S. NAGEL, M. SCHÖNE, AND I. STEPHAN
Zentralinstitut für Kernforschung, Rossendorf
German Democratic Republic

ABSTRACT

An automated measuring system based on a new-developed multi-component wire activation detector (MWAD) is presented which has been applied for neutron spectrometry inside WWER. The MWAD consisting of Au, Mn, Mo, Ni, and W is designed to determine the neutron spectrum in the thermal, epithermal and fast energy region by a single gamma-ray spectrum measurement. Investigations were carried out within an ordinary fuel assembly of the Greifswald NPS (WWER-440) as well as in an experimental fuel assembly of the Rheinsberg NPS (WWER-70). The evaluation of the measurements was done with the new-developed adjustment code COSA based on the generalized least square method.

1. *INTRODUCTION*

Knowledge of the neutron spectrum in a nuclear power reactor is steadily gaining greater importance from the point of view of reactor physics calculation and safety predictions. Nowadays it is generally accepted that sophisticated neutron spectrum measurements inside and outside power reactors can increase the economic rates of the reactor and the reliability of reactor material components. A precise determination of spectral parameters of the neutron field makes it possible to enlarge the accuracy of the fixed installed in-core detectors for power distribution measurements and to improve the radiation damage estimates of the reactor pressure vessel.

Up to now, measurements of the neutron field in power reactors have mainly been carried out with the multiple foil activation method. The axial flux profile has been determined with activation wires. In order to make these measurements simpler and faster a new system was developed by combining the multiple foil technique with the activation wire method.

On the basis of a multi-component wire activation detector (MWAD) a travelling system [1] was designed to measure the axial neutron flux as well as its spectral distribution in WWER-type pressurized water reactors. The system has been applied at the Greifswald NPS (WWER-440) to study the changes of in-core neutron spectrum during normal reactor operation [2] as well as at the Rheinsberg NPS (WWER-70) to investigate the neutron spectrum in an experimental fuel assembly under reduced coolant flow [3].

2. MULTI-COMPONENT WIRE ACTIVATION DETECTOR

The MWAD represents an alloy of different metals appropriate to measure neutrons in a broad energy region. Comparing with commonly used activation foils the MWAD offers the advantage to determine simultaneously several reaction rates with one probe exposition and one gamma-ray spectrum measurement.

The choice of an appropriate MWAD is closely connected with the PWR conditions. Materials in the MWAD should meet the known demands on usual foils such as responsible to different neutron energies and special criteria like the following ones: (i) Detector materials should be homogeneously alloyable to a wire, (ii) the alloyed wire has to be resistant to corrosion and temperatures up to 700 K, (iii) reaction products should have simple decay schemes and small half-lives (for reusing).

Taking these requirements into account a first version of a multi-component detector with the basic material nickel alloyed with gold, manganese and tungsten has been produced. But as a result of the mechanical tests and the metallographic investigations it could be stated that this version didn't meet the requirement at the PWR. The coarse-crystalline microstructure was essentially deformed during the mechanical tests leading to changes of the cross-section and the length of the wire.

These insufficiencies were overcome in a second version by remelting, adding of the hardening component molybdenum to the alloy and cold forming. The final composition of this MWAD with a diameter of 0.9 mm is given in Table 1. Metallographic investigations of the wire showed an essentially finer microstructure in the outer region compared with the first version. Consequently, the abrasive wear was smaller. On the other hand coarse-crystalline zones in the centre of the wire

Table 1

Composition and reactions of the MWAD

Element	Mass fraction [%]	Reaction
Gold	0.30 ± 0.01	$^{197}Au(n,\gamma)^{198}Au$
Manganese	0.34 ± 0.01	$^{55}Mn(n,\gamma)^{56}Mn$
Molybdenum	14.68 ± 0.08	$^{98}Mo(n,\gamma)^{99}Mo$
		$^{100}Mo(n,\gamma)^{101}Mo \rightarrow ^{101}Tc$
Nickel	81.96 ± 0.10	$^{58}Ni(n,p)^{58}Co$
Tungsten	2.44 ± 0.05	$^{186}W(n,\gamma)^{187}W$

guarantee a sufficient bending strength. At a degree of deformation of 75 % the mechanical properties of the MWAD can be characterized by the following parameters: tensile force 1052 N, modulus of rupture 1618 Mpa, and fracture strain 12.3 %. The homogeneity of the wire was proved with activation analysis methods.

3. MEASURING EQUIPMENT ON THE PWR

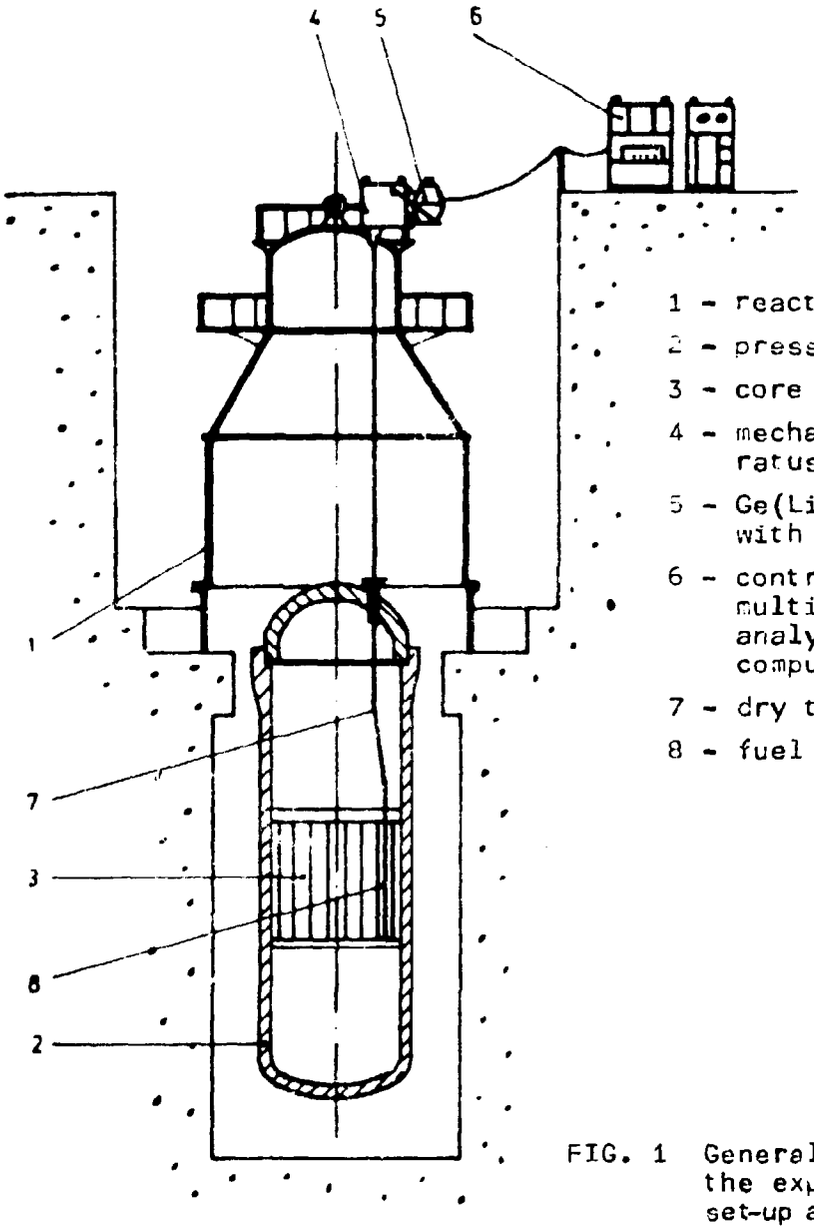

1 - reactor shielding
2 - pressure vessel
3 - core
4 - mechanical apparatus
5 - Ge(Li)-detector with Dewar vessel
6 - control unit, multi-channel analyser, mini-computer
7 - dry tube
8 - fuel assembly

FIG. 1 General scheme of the experimental set-up at WWER-70

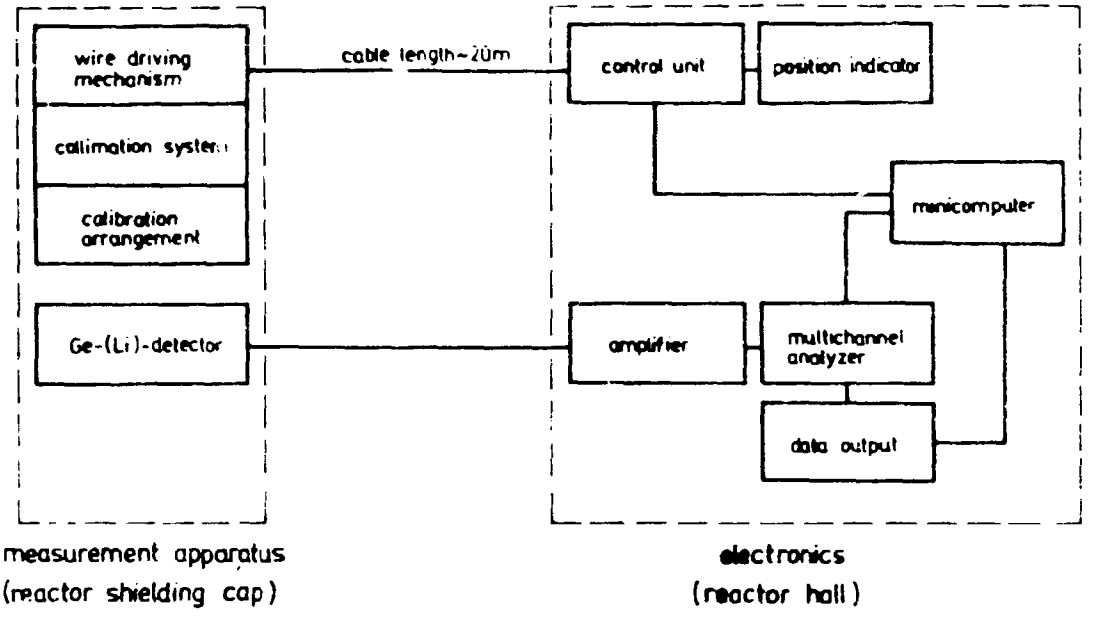

FIG. 2 Block scheme of the measurement equipment

The measuring system consists of the components mechanical apparatus, control unit, gamma-ray spectrometer and minicomputer. A general scheme of the experimental set-up is shown in Fig. 1. The block scheme of the equipment (Fig. 2) gives the connections between the different units.

The mechanical apparatus and the Ge(Li)-detector are installed on the top of the reactor shielding. For measurements the MWAD is driven into the core within a small tube installed in a dry channel of the reactor. After irradiation and cooling the activated part of the wire of 2.5 m length is measured within the mechanical apparatus. The inner build-up of the mechanical apparatus is shown in Fig. 3. The different parts are arranged in four levels within a tight casing. The wire drum with drive is situated on the upper level for "Lifting" the wire at two different speeds. On the second level, the drive mechanism for "Sinking" is arranged using friction wheels. All movements are started from the control unit. The position indicator (angle measuring system from Carl Zeiss Jena) being on the third level has precisely and non-fugitively to measure the wire position. The reference point for the position indication is the lower edge of the wire. The position calibration is done with a photoelectric barrier (uncertainty about 1 mm).

The activity calibration is performed using a ^{137}Cs standart source which has approximately the same geometry and activity like the MWAD part seen by the Ge(Li)-detector through the collimator. The collimator is situated in the lowest level. It has an aperture of 10 x 10 mm and a length of 380 mm. To decrease the gamma-ray intensity falling on the Ge(Li)-detector lead absorbers can be inserted. The detector

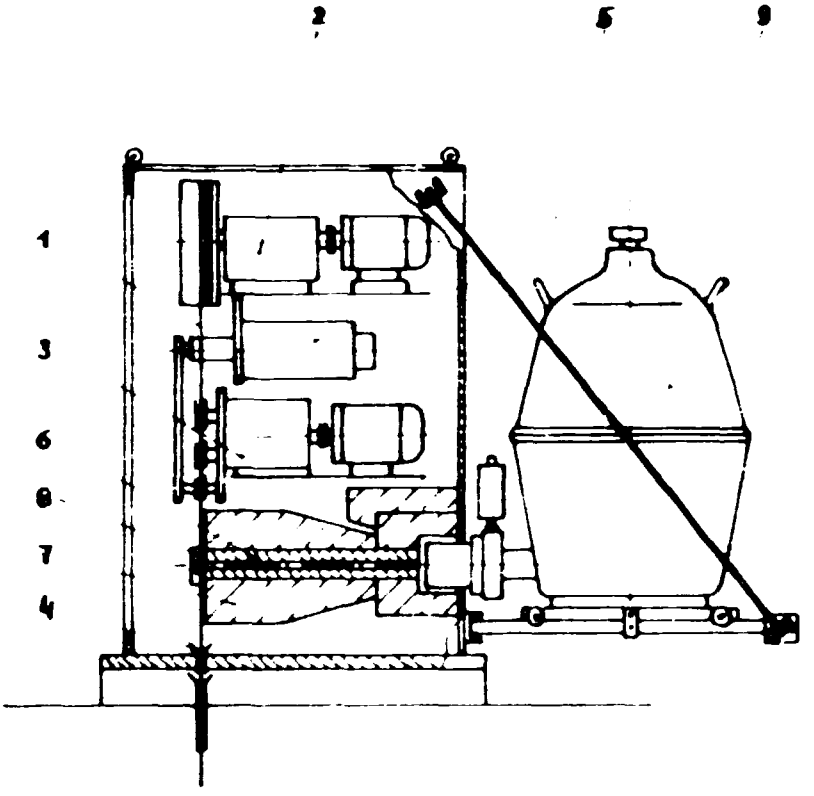

FIG. 3 Schematic build-up of the mechanical apparatus

1 - MWAD, 2 - wire drum with drive, 3 - drive mechanism, 4 - wire insertion, 5 - position indicator, 6 - collimator, 7 - detector shielding, 8 - position and activity calibration equipment, 9 - Ge(Li)-detector with pre-amplifier and Dewar vessel

shielding has to reduce the influence of the background radiation and the activity of the wire which is not situated in front of the collimator.

The control unit (Fig. 2) connected with the mini-computer has to control all movements of the wire. It can be done by hand or with an automated programme. There are three programmes for (i) irradiation, (ii) measuring step by step, and (iii) measuring continuously. The activity of the irradiated wire is determined with the Ge(Li)-detector using a multichannel analyser of the type NTA-1024. The mini-computer controls the multichannel analyser and evaluates the gamma-ray spectra.

4. EVALUATION

The evaluation of the measurements is performed in two steps. The first step is done on the spot using the EMG-666/B mini-computer. The peak areas of the gamma-ray spectrum are determined with standard summing procedure. From the peak area P_i the reaction rate R_i is computed corresponding the formula

$$R_i = \frac{P_i}{I_i \cdot G_i \cdot m \cdot L/A_i \cdot t_{m,eff} \cdot \gamma_i \cdot \varepsilon_a \cdot \varepsilon_i \cdot S_i} \prod_{l=1}^{4} k_i^{(l)}$$

where

I_i - isotopic mole fraction, G_i - mass fraction of the element in the MIAD, m - mass, L - Avogadro's number, A_i - relative atomic mass, $t_{m,eff}$ - measuring time (life-time) γ_i - gamma-ray emission probability, ε_a - absolute efficiency, ε_i - relative efficiency, S_i - factor for gamma-ray self-absorption.

The factors $k_i^{(l)}$ are defined as follows

$k_i^{(1)} = e^{\lambda_i \cdot t_c}$ with λ_i - decay constant, t_c - cooling time,

$k_i^{(2)} = 1/(1 - e^{-\lambda_i \cdot t_r})$ with t_r - irradiation time,

$k_i^{(3)} = \lambda_i t_m/(1 - e^{-\lambda_i \cdot t_m})$ with t_m - measuring time (clock time),

$k_i^{(4)}$ - additional corrections for ^{101}Tc and ^{58}Co due to complicated decay.

The absolute efficiency is determined from the gamma-ray peak of the standard source ^{137}Cs corresponding

$$\varepsilon_a = \frac{P_c}{a \cdot \gamma_c \cdot t_{m,eff}} ,$$

where c indicates the calibration and a stands for the activity of the standard source. If we insert ε_a into the equation for R_i the life-time $t_{m,eff}$ drops out.

Summarizing the factors not depending on the nuclide to

$$C = \frac{\gamma_c}{P_c} \cdot \frac{a}{m} \cdot \frac{1}{L} ,$$

we can write for the reaction rate

$$\kappa_i = \frac{P_i \cdot A_i \cdot C}{\gamma_i \cdot I_i \cdot G_i \cdot \varepsilon_i \cdot S_i} \cdot \prod_{l=1}^{4} k_i^{(l)}$$

On the base of the reaction rates some parameters of the neutron field like thermal and fast neutron flux as well as neutron spectrum hardness are calculated using the following formulae:

The neutron spectrum hardness α defined by

$$\alpha = \varphi_e / \phi_t$$

where φ_e - epithermal neutron flux per unit lethargy,
ϕ_t - thermal neutron flux,

is the mean value between α(Au/Mn) and α(W/Mn), where α(Au/Mn) and α(W/Mn) are calculated from the ratios of the reaction rates R(Au)/R(Mn) and R(W)/R(Mn), respectively:

$$\alpha(\mathrm{Au/Mn}) = \frac{\frac{\sqrt{\pi}}{2}\sqrt{\frac{T_0}{T}}\left(1 - \frac{R(\mathrm{Au})}{R(\mathrm{Mn})} \Big/ \frac{\sigma_0(\mathrm{Au})}{\sigma_0(\mathrm{Mn})}\right)}{\left(\frac{R(\mathrm{Au})}{R(\mathrm{Mn})} \Big/ \frac{\sigma_0(\mathrm{Au})}{\sigma_0(\mathrm{Mn})}\right)\frac{I(\mathrm{Mn})}{\sigma_0(\mathrm{Mn})} - \frac{I_0(\mathrm{Au})}{\sigma_0(\mathrm{Au})}}$$

with T - neutron temperature (T_0 = 293 K), σ_0 - thermal activation cross section, I - resonance integral.

By using the effective thermal activation cross section

$$\sigma_{\mathrm{eff,t}} = \frac{\sqrt{\pi}}{2}\sqrt{\frac{T_0}{T}}\,\sigma_0 + \alpha \cdot I$$

the thermal flux is calculated from the reaction rates of Au, W, and Mn:

$$\phi_t = \frac{R}{\sigma_{\mathrm{eff,t}}} \cdot$$

The fast neutron flux is derived from the reaction rate of ^{58}Ni

$$\phi_f = \frac{R(^{58}\mathrm{Ni})}{\langle\sigma\rangle \cdot K}$$

with $\langle\sigma\rangle$ - cross section averaged over a fission neutron spectrum,
K - correction factor for the decay of ^{58}Co [4].

By the help of this in-field evaluation the experimental results can be estimated immediately after having closed the accumulation of the gamma-ray spectra. Furthermore, the staff of the NPS can be informed with rough, but up to date neutron field data.

The second step of the measurement evaluation is performed off-line using a new-developed adjustment code, named COSA (Correction of spectra using activation measurements) [5]. This code is similar to STAY'SL [6] and other codes based on the generalized least squares method. COSA1, the first version of this code, uses measured activation rates and calculated neutron flux spectra together with corresponding covariance data in order to obtain the most probable adjusted spectra, derived integral quantities and corresponding new covariance data. Cross section covariances are not yet accounted for. A test of COSA1 on REAL-80 benchmark data shows a very close agreement with published average results of the REAL-80 participants [7].

5. RESULTS

In the following some selected results of our measurements with the MWAD are presented to illustrate the possibilities of the measuring system. A typical gamma-ray spectrum is shown in Fig. 4. The single peaks at 412 keV(^{198}Au), 480 keV and 686 keV(^{187}W), 740 keV(^{99}Mo), 811 keV(^{58}Co), and 847 keV(^{56}Mn) were used for calculating the reaction rates. The gamma-ray peak at 662 keV is caused by the calibration standard ^{137}Cs.

At the WWER-440 the measurements were carried out during the fourth cycle of unit four in monthly intervals. To compare directly the experimental data with theoretical values the axial measuring positions were chosen in correspondence with the points of the reactor physics calculation. Table 2 contains the reaction rates at the measuring position No. 8 for the nine measuring periods during the fourth cycle. The axial fine structure of the thermal neutron flux and the spectrum hardness around the measuring position No. 7 and 8 is shown in Fig. 5 measured in steps of 1 cm. Due to the influence of the distance grid the thermal flux is reduced in the surrounding of the grid. On the other hand, the spectrum hardness α is increased in this disturbed region. Because of the above mentioned reason the measuring points were not chosen directly between the distance grids, but it can be seen from Fig. 5 that they avoid the influence region of the grids.

An example of first experience with spectrum adjustment using the code COSA1 is given in Fig. 6 and Table 3.

The calculations had been performed using the REAL-80 100 energy group structure and REAL-80 cross section data. For the reactions ^{98}Mo(n,γ) and ^{100}Mo(n,γ) group cross sections had been derived from the ENDF/B5 fission product file with help of the programs RECENT and FEDGROUP. The input spectrum was taken from 69-group cell calculations with the WIMS-code.

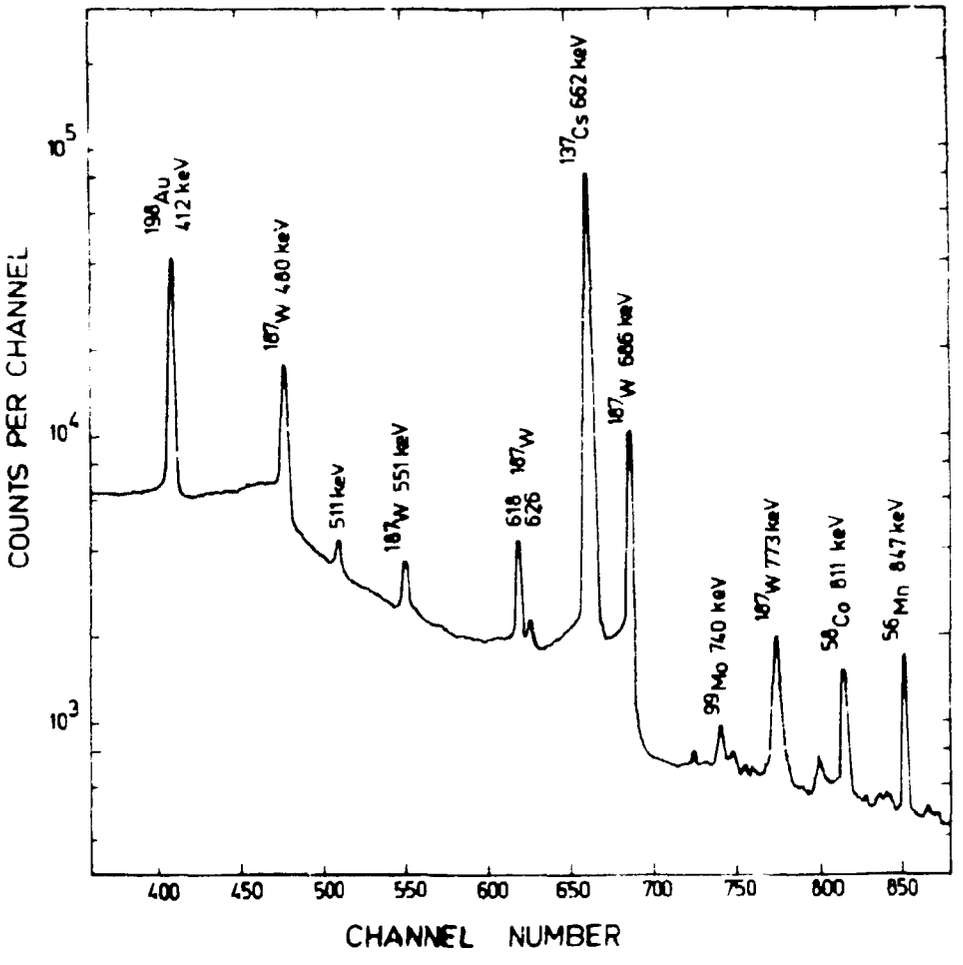

FIG. 4 Gamma-ray spectrum of the MWAD

Table 2

Reaction rates at the measuring position No. 8, corresponding a distance from the lower core edge of 182 cm, for unit 4 of the Greifswald NPS

measuring period	effective days	^{55}Mn [$10^{-10}s^{-1}$]	^{58}Ni [$10^{-11}s^{-1}$]	^{98}Mo [$10^{-11}s^{-1}$]	^{100}Mo [$10^{-11}s^{-1}$]	^{186}W [$10^{-9}s^{-1}$]	^{197}Au [$10^{-8}s^{-1}$]
I	18	3.49	0.799	6.27	3.96	3.53	1.16
II	37	3.70	0.679	6.62		3.96	1.27
III	78	3.84	1.00	6.92	5.13	4.00	1.31
IV	104	3.57	0.913	6.41	4.69	3.79	1.23
V	131	4.16	1.04	7.00	5.20	4.46	1.42
VI	171	3.98	0.715	6.00	4.88	4.06	1.30
VII	215	3.59	1.04	6.86	4.79	3.92	1.26
VIII	240	4.44	1.08	8.75	5.60	4.63	1.47
IX	267	4.39	0.881	8.30	5.58	4.64	1.47

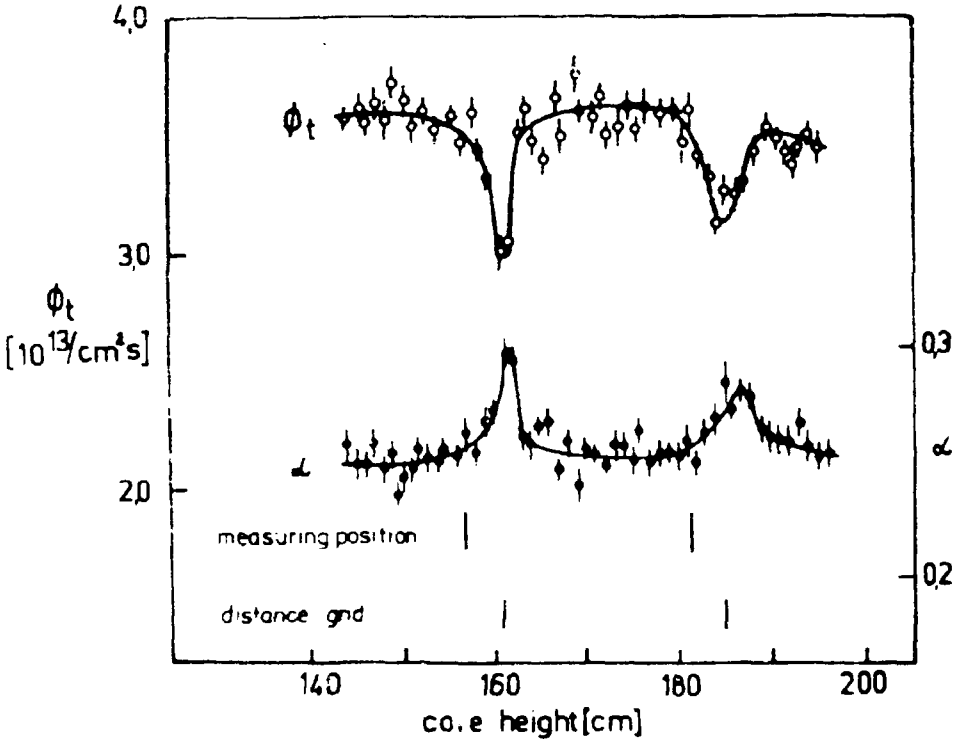

FIG. 5 Fine structure of the thermal neutron flux and the spectrum hardness

Table 3

Integral fluxes and their relativ standard deviations for unadjusted and adjusted spectra corresponding to Fig. 6

	unadjusted spectrum		adjusted spectrum	
	flux [10^{14} n/cm² s]	error [%]	flux [10^{14} n/cm² s]	error [%]
ϕ total	2.907	22.4	3.122	13.6
ϕ E > 0.5 eV	2.492	23.7	2.666	14.5
ϕ E > 0.1 MeV	1.323	33.5	1.401	25.8
ϕ E > 1.0 MeV	0.641	43.0	0.683	22.9

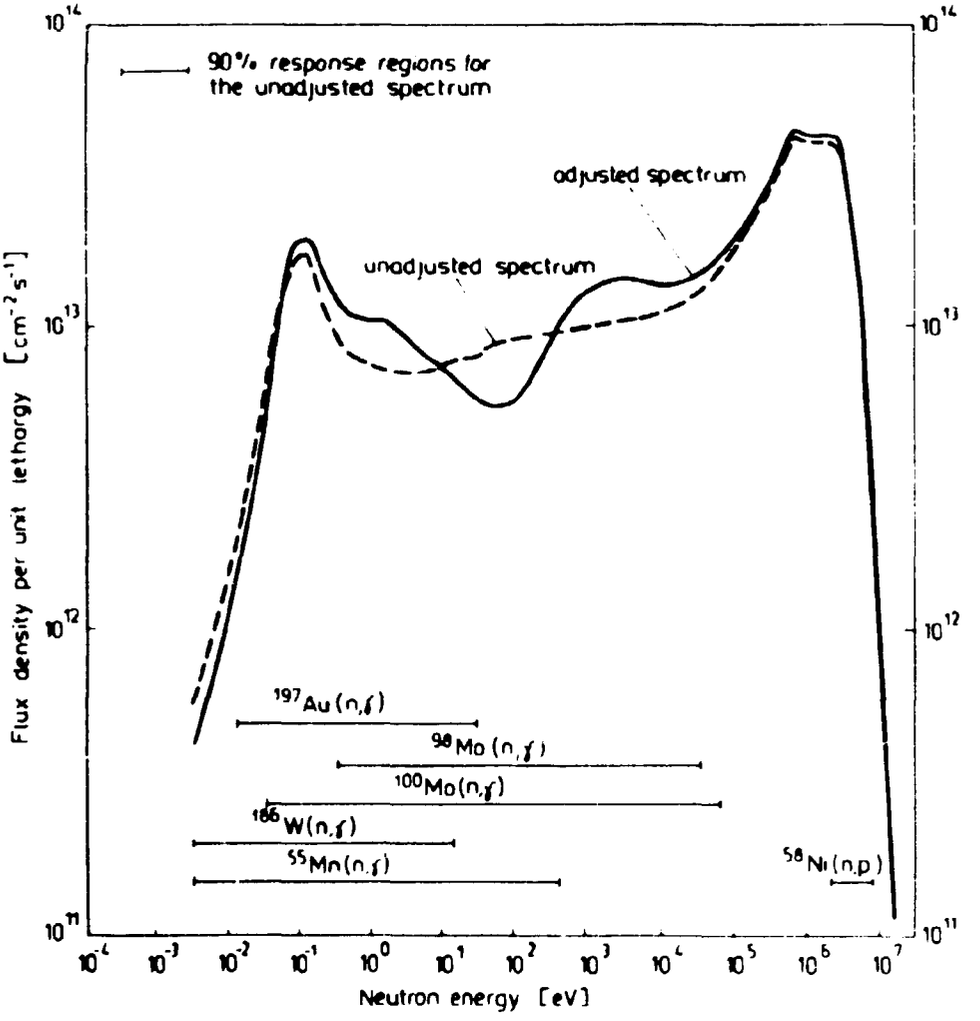

FIG. 6 Example of an unadjusted and adjusted neutron spectrum for the WWER-440

The spectrum was assumed to have a relative standard deviation of 0.5 for all groups with exception of the first two and the last twelve. Large positive correlations for adjacent spectrum groups had been introduced, to avoid unreasonable resonance structure in the adjusted spectrum caused by resonance detectors. The calculation of reaction rates covariances is described in Section 6.

The 90 % response regions for the available six activation reactions given in Fig. 6 show, that a substantial part of the spectrum is not represented by the measurement. Nevertheless the adjustment gives a physically reasonable spectrum (Fig. 6) reproducing the measured activation values within their error boundaries.

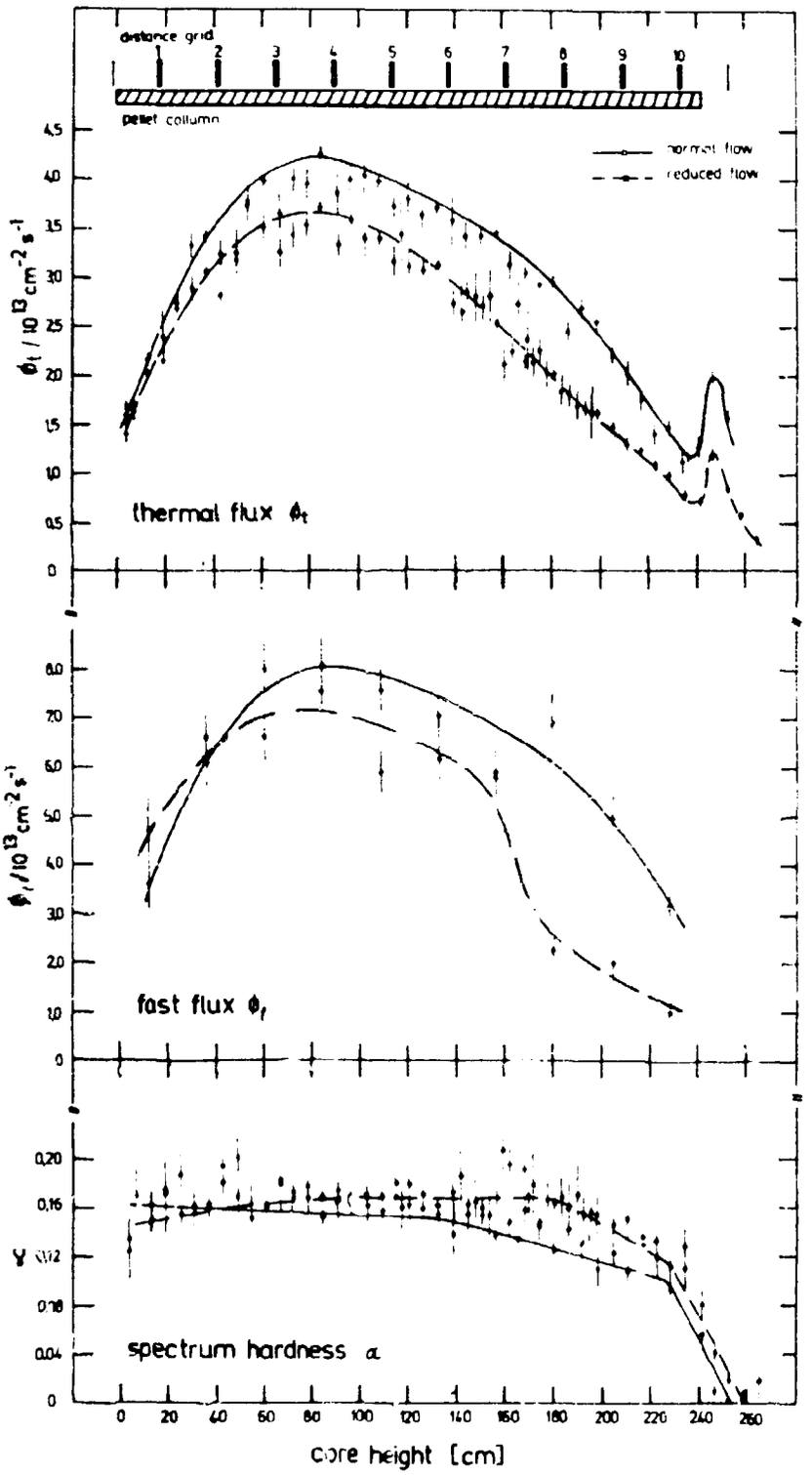

FIG. 7 Axial neutron flux distribution in the experimental assembly of the VVER-70 at reduced coolant flow rate

In Table 3 some flux integrals and their relative standard deviations are given for the spectra shown in Fig. 6. The relatively large errors even after adjustment can be explained by the large input spectrum errors in connection with incomplete coverage of the energy region by detector reactions.

For investigating abnormal occurences we mounted the measuring system at the Rheinsberg NPS (WWER-70) to measure within an experimental fuel assembly the neutron spectrum at different coolant flow states. In Fig. 7 the axial distribution of the thermal and fast neutron flux as well as the spectrum hardness is presented for normal operation conditions and for minimum coolant flow rate of 26 %. It can be seen that due to the reduced coolant flow the neutron fluxes and spectrum hardness is especially changed in the upper core region. The thermal and fast neutron flux is decreased while the spectrum hardness is increased. By using this effect it is in principle possible to control coolant boiling in extraordinary situations at water cooled reactors.

6. ERROR PROPAGATION STUDY

In the following an error propagation study is carried out. To generate the covariances of the experimental data we follow the recommendations of ref. [8]. We consider only relative uncertainties of the different quantities δR_i, δP_i etc. Then, the covariance matrix of the reaction rates can be expressend

$$\begin{aligned} \mathrm{Cov}(R_i,R_j) &= \langle \delta R_i\, \delta R_j \rangle \\ &= \langle \delta P_i\, \delta P_j \rangle + \langle \delta \gamma_i\, \delta \gamma_j \rangle + \langle \delta I_i\, \delta I_j \rangle + \langle \delta G_i\, \delta G_j \rangle \\ &\quad + \langle \delta \varepsilon_i\, \delta \varepsilon_j \rangle + \langle \delta S_i\, \delta S_j \rangle + \langle \delta C_i\, \delta C_j \rangle + \sum_{l=1}^{4} \langle \delta k_i^{(l)}\, \delta k_j^{(l)} \rangle \quad , \end{aligned}$$

where the symbol $\langle f \rangle$ is used for the expected value of the quantity f. We have here assumed that no vertical correlations occur which means that terms of the form $\langle \delta P_i\, \delta \gamma_i \rangle$, $\langle \delta P_i\, \delta I_i \rangle$ etc. do not exist. The relation between the correlation and covariance matrix is the following

$$\mathrm{Cov}(R_i,R_j) = \langle \delta R_i\, \delta R_j \rangle = \mathrm{Corr}(R_i,R_j) \sqrt{\langle \delta R_i\, \delta R_i \rangle} \cdot \sqrt{\langle \delta R_j\, \delta R_j \rangle}.$$

Table 4 contains the main sources of errors and its correlation. The uncertainties δP_i are considered as being independent, i.e. systematic uncertainties which would establish correlations are neglected in comparison with the statistical one. The $\delta \gamma_i$, δI_i and a part of the δG_i are also independent. The calibration factor is for all nuclides the same and consequently the δC_i show full correlation. For estimating the uncertainties and correlations of the time factors

Table 4

List of the uncertainty components [%]

quantity	^{55}Mn	^{58}Ni	^{98}Mo	^{100}Mo	^{186}W	^{197}Au	remarks
number	1	2	3	4	5	6	
δP_i	2.0	5.3	8.4	2.7	2.0	1.6	counting statistics
$\delta \varepsilon_i$	0.3	0.3	0.5	4.0	0.4	0.02	literature [9]
δI_i	0	0.02	0.04	0.1	0.35	0	literature [9]
δG_i	2.4	0.1	0.5[a]	0.5	2.0	2.7	certificate MWAD
$\delta \varepsilon_i$	1.4[b]	1.5[b]	1.6[b]	2.5[b]	1.9[b]	2.2[b]	own measurements
δS_i	0.6[c]	0.6[c]	0.6[c]	0.6[c]	0.6[c]	0.6[c]	
δC_i	2.6[d]	2.6[d]	2.6[d]	2.6[d]	2.6[d]	2.6[d]	certificate of the standard
$\delta k_i(1)$	0.1[e]	0.1[e]	0.1[e]	0.7[e]	0.1[e]	0.1[e]	estimations with uncertainties
$\delta k_i(2)$	1.0[f]	1.0[f]	1.0[f]	1.2[f]	1.1[f]	1.0[f]	of the half-lives of ref. [9]
$\delta k_i(3)$	0.2[e]	0.3[e]	0.1[e]	1.4[e]	0.1[e]	0.1[e]	
$\delta k_i(4)$	0	2.5	0	3.0	0	0	

[a] $Corr(G_3, G_4) = 1.00$ fully correlated (same element)

[b] $Corr(\varepsilon_i, \varepsilon_j) = 0.80$ corresponding estimations in ref. [8]

[c] $Corr(S_i, S_j) = 0.70$ caused to common uncertainties in the gamma-ray attenuation cross sections

[d] $Corr(C_i, C_j) = 1.00$ fully correlated (calibration factor)

[e] uncorrelated, because this uncertainty is mainly caused by the uncertainty of the λ_i

[f] strong correlation:

$$Corr(\delta k_i^{(2)}, \delta k_j^{(2)}) = \begin{pmatrix} 1.00 & & & & & \\ 0.99 & 1.00 & & & & \\ 0.96 & 0.95 & 1.00 & & & \\ 0.82 & 0.82 & 0.78 & 1.00 & & \\ 0.93 & 0.92 & 0.89 & 0.76 & 1.00 & \\ 0.99 & 0.99 & 0.96 & 0.82 & 0.93 & 1.00 \end{pmatrix}$$

$\delta k_i^{(1)}$ the values $\delta t_c = \delta t_m = 0$ and $\delta t_r = 1$ % were assumed.

The final results of the error propagation study are summarized in Table 5. It can be seen that the thermal neutron fluxes from different reaction rates are relatively strong correlated so that an averaging over the different values does not essentialy reduce the uncertainty. The correlations of the reaction rates are used for the adjustment code COSA.

7. FINAL REMARKS

For the present purpose, only some results from our in-core measurements at the water cooled reactors WWER-70 and WWER-440 have been quoted to demonstrate the possibilities of the measuring system. The design of the hardware and software is suf-

Table 5

Relative standard deviation and correlation matrix of the reaction rates and some parameters of the neutron field

quantity	rel. standard dev. [%]	correlation matrix
R_1	4.5	1.00
R_2	6.7	0.32 1.00
R_3	9.1	0.24 0.16 1.00
R_4	7.1	0.63 0.23 0.18 1.00
R_5	4.5	0.50 0.34 0.26 0.37 1.00
R_6	4.8	0.49 0.33 0.25 0.37 0.53 1.00
$\alpha\ (R_5/R_1)$	13.6	1.00
$\alpha\ (R_6/R_1)$	10.0	0.48 1.00
$\phi_t(R_1)$	8.3	1.00
$\phi_t(R_5)$	8.5	0.85 1.00
$\phi_t(R_6)$	9.8	0.92 0.67 1.00
$\phi_f(R_2)$	8.4	

ficiently general that the MWAD at present used can be replaced with another type of detector, which is e.g. more responsible for the fast neutron energy region. Then, measurements of the neutron field immediately at or near the reactor pressure vessel can be carried out to improve the radiation damage estimates. The measuring system gives here the advantage to investigate directly the temporal and axial changes of the neutron spectrum, a work which can be hardly performed with the conventionally used multiple foil technique.

REFERENCES

[1] MEHNER, H.-C., DENNSTÄDT, I., HAGEMANN, U., NAGEL, S., SCHÖNE, M., Kernenergie 25 (1982) 334

[2] MEHNER, H.-C., NAGEL, S., SCHÖNE, M., STEPHAN, I., HAGEMANN, U., PIEPER, U., GEHRIG, W., Application of the multi-component wire activation detector system for in-core neutron spectrometry at a NPS, paper presented at Fifth ASTM-EURATOM Symposium on Reactor Dosimetry, Geesthacht, FRG, Sept. 24 - 28, 1984

[3] HAGEMANN, U., MEHNER, H.-C., In-core neutron spectrometry at reactors of WWER types, IAEA Seminar on Diagnosis of and Response to Abnormal Occurences at Nuclear Power Plants, Dresden, GDR, June 12 - 15, 1984

[4] DENNSTÄDT, I., MEHNER, H.-C., Rep. ZfK-449, Zentralinstitut für Kernforschung, Rossendorf (1981)

[5] BÖHMER, B., Code COSA, to be published

[6] PEREY, F.G., Rep. ORNL-TM-6062, Oak Ridge National Laboratory (1977)

[7] ZIJP, W.L. et al., Rep. ECN-128, Netherlands Energy Research Foundation, Petten (1983)

[8] MANNHART, W., Rep. PTB-FMRB-84, Physikalisch-Technische Bundesanstalt (1981)

[9] ZIJP, W.L., BAARD, J.H., Rep. ECN-70, Netherlands Energy Research Foundation (1979)